GEOLOGICA CARPATHICA, 50, 3, BRATISLAVA, JUNE 1999
257–272

DIAGENETIC TRIOCTAHEDRAL PHYLLOSILICATES FROM SEDIMENTS OF THE ŠAMBRON ZONE (EASTERN SLOVAKIA): XRD, SEM, AND EMPA STUDY

ADRIAN BIROŇ*, JÁN SOTÁK and JURAJ BEBEJ

Geological Institute, Slovak Academy of Sciences, Bratislava; Branch: Severná 5, 974 01 Banská Bystrica, Slovak Republic;
*biron@gu.bb.sanet.sk

(Manuscript received March 24, 1998; accepted in revised form March 17, 1999)

Abstract: Trioctahedral clay minerals occurring as phyllosilicate cement in diagenetically altered serpentinitic graywackes have been studied using X-ray powder diffraction, scanning electron microscopy, and microprobe analyses. Two distinct cement assemblages were observed: (1) saponite ± calcite ± dolomite ± opal-CT ± pyrite, which is restricted to quartz-rich graywackes, and (2) ordered mixed-layered chlorite/smectite (C/S) + saponite ± calcite ± dolomite ± opal-CT ± pyrite characteristic of serpentinite-rich graywackes. Swelling properties as well as chemical analyses reveal a predominance of high-charge layers both in saponite and C/S. Saponite and C/S show a unique composition of 2 : 1 layers with respect to Si/(Si + Al) ratio. The decrease in Mg/(Mg + Fe) ratio from saponite to C/S with respect to the increasing Al^{IV} content implies that Fe-Mg substitution was controlled by distortion of tetrahedral sheets caused by Si-Al substitution. The lack of correlation between whole-rock and phyllosilicate Mg/(Mg + Fe) ratios supports this interpretation. Textural as well as compositional evidence suggests that both saponite and C/S originated by the interaction of the sediment with pore-fluids during burial as direct precipitates. It is inferred that a different bulk rock composition, and consequently, a different chemistry of pore-fluids played an important role during authigenesis. Particularly, the availability of Al may have been a primary factor controlling whether saponite or C/S formed, while the role of Mg (or Mg/(Mg + Fe) ratio) as well as the role of temperature were only of secondary importance.

Key words: Šambron Zone, serpentinitic sandstones, diagenesis, saponite, mixed-layer chlorite/smectite, corrensite.

Introduction

Trioctahedral clay minerals such as saponite and corrensite (1 : 1 regularly interstratified chlorite/smectite) are abundant in diverse geological settings. They widely form under diagenetic to subgreenschist facies conditions in regionally metamorphosed and hydrothermally altered mafic igneous rocks (e.g. Kristmannsdóttir 1978; Bettison & Schiffman 1988; Shau et al. 1990; Schiffman & Fridleifsson 1991; Shau & Peacor 1992; Robinson et al. 1993; Schiffman & Stautigel 1995), evaporite and carbonate sequences (e.g. April 1981; Bodine & Madsen 1987; Fisher 1988; Janks et al. 1992; Masaryk et al. 1995), or clastic sedimentary rocks containing significant amounts of mafic volcanoclastic material (e.g. Iijima & Utada 1971; Galloway 1974; Almon et al. 1976; Helmond & van de Kamp 1984; Inoue et al. 1984; Chang et al. 1986; Inoue & Utada 1991; Bautier et al. 1995). In all the above mentioned environments, the origin of chlorite/smectite minerals is related to high concentrations of Mg. Corrensite generally occurs as an intermediate product during the smectite-to-chlorite transition. Most commonly, this transition occurs through the discontinuous sequence of three phases saponite, corrensite, and chlorite, concurrent with increasing temperature of formation (e.g. Inoue & Utada 1991; Meunier et al. 1991; Schiffman & Stautigel 1995). Only a few examples have been interpreted as a more or less continuous series of mixed-layer chlorite/smectite minerals (Schultz 1963; Helmond & van de Kamp 1984; Chang et al. 1986). Alternatively, a direct precipitation of corrensite from concentrated solution (without saponite precursor) has also been reported (Almon et al. 1976; Shau et al. 1990; Bettison-Varga et al. 1991; Bautier et al. 1995).

This study is concerned with saponite and corrensite-like chlorite/smectite mixed layer (C/S) clay from serpentinitic sandstones of the flysch formations of the Šambron Zone of the Central Carpathian Paleogene Basin (Levoča sub-Basin) (Soták & Bebej 1996). The sandstones are significantly enriched with unstable lithic components — serpentinized ultramafic rocks. This specific composition gave rise to the formation of mafic expandable clay minerals during burial diagenesis. The exposed sedimentary sequence with serpentinitic sandstones represents a narrow stratigraphic range (only a few meters in thickness), so that physical conditions of post-sedimentary alteration were equal for each sandstone bed. Nevertheless, they show significantly different mineralogy of the authigenic clay phases and individual sandstone beds have either saponitic or corrensitic phyllosilicate cement. Apparently, the conventional scheme of temperature controlled saponite to chlorite series cannot explain such spatial distribution of authigenic assemblages. This indicates, that instead of temperature, other factors influenced the origin of the clay minerals in serpentinitic sandstones from the Šambron Zone.

In this paper, it is our intention to: (1) demonstrate the occurrence, structure and chemistry of saponite and C/S; and (2) propose a model that explains their formation in the serpentinitic sandstones of the Šambron Zone.

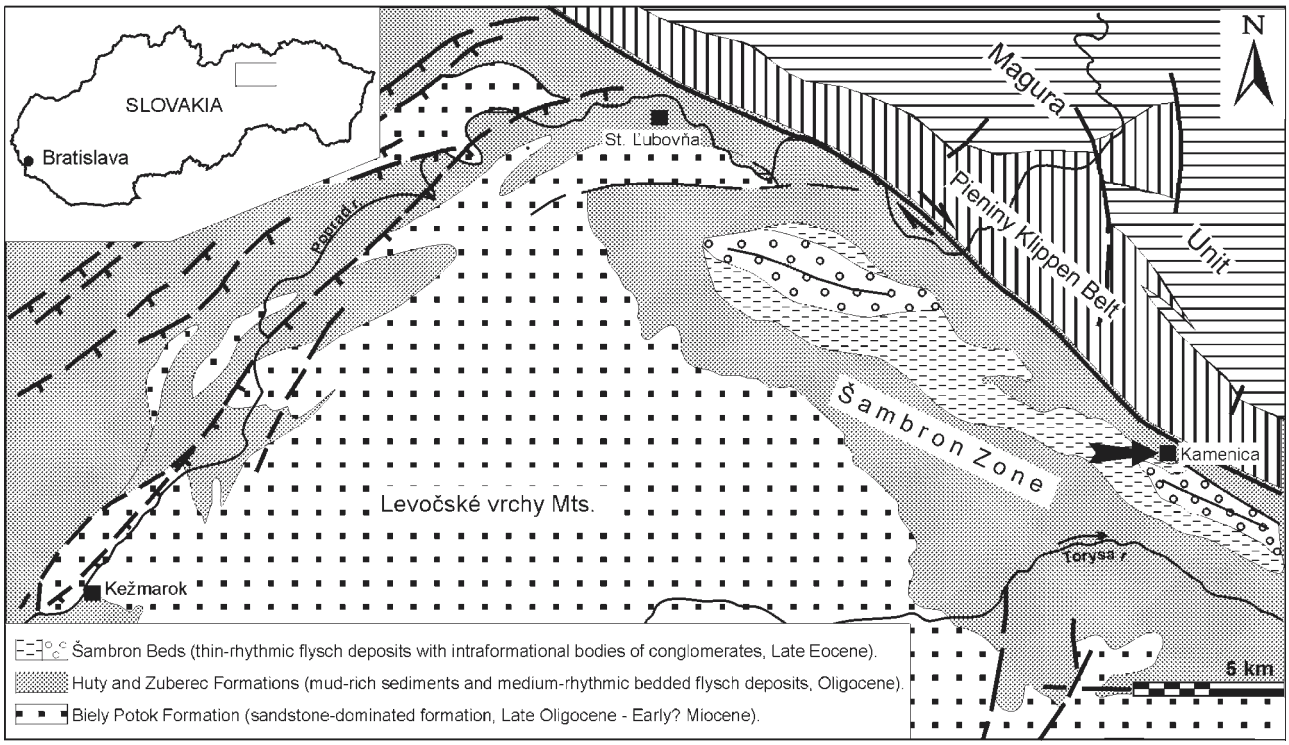

Fig. 1. Geological sketch-map of the Levočské vrchy Mts. depicting the location of serpentinitic sandstone occurrences near the junction of the Central Carpathian Paleogene with the Pieniny Klippen Belt (westwards of Kamenica village, black arrow).

Geological setting

The serpentinitic graywackes were found in the Šambron Zone of the Central Carpathian Paleogene in Eastern Slovakia (localities near Kamenica — Fig. 1; Soták & Bebej 1996). They occur within a thinly bedded sandstone–claystone sequence resembling the "zebra"-type flysch. The sandstones are grey in colour, fine- to medium grained and usually laminated in Bouma Td intervals. The claystones are weakly calcareous (average content of CaO and MgO in carbonate fraction is 5.12 and 3.68 wt. %, respectively) and with their brownish colour close to the Menilite shales. The sandstone–claystone sequence is also interbedded with thin layers of whitish dolomites. The age corresponds to the Late Oligocene (NP 24–25 nanoplanktone zone; Soták & Bebej 1996). The graywacke flysch deposits near Kamenica are refolded into recumbent to moderately plunging folds and intersected by overthrust faults. The occurrence of serpentinite-rich flysch deposits in the Šambron Zone indicates a suture zone of the Tertiary collision running along the junction of the Central Carpathian Paleogene with the Pieniny Klippen Belt. The Šambron Zone is thought to be a perisutural part of the Central Carpathian Paleogene Basin enriched with ophiolitic detritus.

Analytical methods

Samples were examined by the following methods: optical microscopy, X-ray powder diffraction (XRD), scanning electron microscopy (SEM), back-scattered electron imaging (BSE). The chemical composition of clay minerals was determined by electron microprobe analysis (EMPA) and whole-rock chemical composition by X-ray fluorescence spectrometry.

XRD. Preparation of clay size fractions for XRD analyses utilized standard procedures. Samples were crushed to obtain chips about 5 mm in diameter. Rock fragments were then disaggregated in distilled water using an ultrasonic bath for 10 min to extract phyllosilicates from pore spaces. Suspensions were flocculated with NaCl and subsequently treated with sodium acetate buffer, H_2O_2 and with sodium dithionite to remove carbonate minerals, organic matter and Fe, Mn-oxides, respectively (Jackson 1975). The <2 μm fraction was separated by sedimentation in distilled water. Mg^{2+} and K^+ forms of clay fractions were prepared by exchange (three times, overnight) with 1 M chloride solutions. Finally, clay fractions were repeatedly washed with distilled water, centrifuged to remove excess salts, and then air dried.

Oriented samples for XRD analysis were prepared by sedimentation of a clay suspension on glass slide (10 mg/cm^2) and analyzed in the air dried state and after saturation by ethylene glycol vapour for 8 h at 60 °C. In addition, Mg-saturated clay was also analyzed after solvation with glycerol vapour at 100 °C for 24 h (Reynolds 1988). The K-saturated samples were heated at 550 °C for 1 h and then analyzed. XRD patterns of randomly oriented specimens were also obtained in order to determine the *d(06,33)* value of phyllosilicates. Silicon powder was used as an internal standard.

XRD analyses were performed on a Philips PW 1710 diffractometer (35 kV, 20 mA, CuKα, Ni-filter, divergence slit: 1°, receiving slit: 0.1 mm, range: 2–50°2Θ) and a DRON 2.0 diffractometer (35 kV, 20 mA, CuKα, Ni-filter, divergence

slit: 1 mm, receiving slit: 0.1 mm, range: 1–50°2Θ and 58–63°2Θ). Oriented preparations were scanned at goniometer speed 1°2Θ/min, unorientated powders at 0.5°2Θ/min.

SEM. Specimens for SEM were prepared as freshly fractured, air dried, gold-coated rock fragments or polished, carbon-coated thin sections. Both secondary electron and backscattered electron imaging were employed. SEM observations were carried out on a JEOL JSM 840 scanning electron microscope equipped with energy-dispersive spectrometer and a Tesla BS 300 scanning electron microscope.

EMPA. Quantitative, wavelenght-dispersive analyses of saponite and C/S were performed on a JEOL JXA-733 Superprobe electron microprobe at 15 keV accelerating voltage and 3 nA beam current using an electron beam approximately 3 μm in diameter. The following silicate and oxide standards were used: albite (Na), orthoclase (K), Al_2O_3 (Al), quartz (Si), wollastonite (Ca), MgO (Mg), hematite (Fe), rhodonite (Mn), TiO_2 (Ti) and chromite (Cr). Corrections were made with the ZAF computing program.

Materials

The detailed petrographic description of sandstones has been given by Soták & Bebej (1996). The sandstones are mostly graywackes (Füchtbauer 1959) with lithic grain content between 40 and 80 %. Lithic grains include predominantly fragments of serpentinized ultramafic rocks with the typical mesh and loop textures. The coarse-grained, flaky lizardites and fragments of fibrous chrysotiles are also present. In addition, the detrital framework contains a subordinate proportion of glassy fragments, large detrital flakes of muscovite, biotite or chlorite, carbonate and phyllitic rocks. Intraclasts from the surrounding shales are relatively frequent. Other major detrital constituents are quartz grains (10 to 50 %). Feldspars form only an accessory component of the sandstones (up to 10 %). Both alkali feldspars and plagioclases (Na- or Ca-dominated) are present.

The sandstones contain abundant phyllosilicate cement. Clay minerals are present both as a pore-filling cement, and as an alteration phase in lithic and feldspar grains. Non-phyllosilicate authigenic minerals are volumetrically insignificant and they are not uniformly distributed. Considering detrital modes and cement mineralogy, the sandstones can be divided into two distinct types:

(A) Quartzolithic graywackes with significant content of siliciclastic material ($Q_{37}F_{12}L_{51}$) and authigenic assemblage: saponite and subordinate dolomite, calcite, opal-CT and pyrite.

(B) Lithic graywackes with absolute prevalence of the lithic component ($Q_{19}F_7L_{74}$) and authigenic assemblage: C/S + saponite and subordinate dolomite, calcite, opal-CT and pyrite.

The average whole-rock chemical compositions are shown in Table 1.

Table 1: Whole-rock chemical analyses of serpentinitic graywackes.

Type	Quartzolithic graywackes			Lithic graywackes		
Mean detrital mode	$Q_{37}F_{12}L_{51}$			$Q_{19}F_7L_{74}$		
Sample	258/V	K-I	255/II	256/TM1		
SiO_2	56.42	59.65	49.50	47.70	47.80	47.60
Al_2O_3	7.08	7.83	7.72	10.62	11.55	10.06
MgO	11.98	8.40	14.47	16.68	14.31	11.39
Fe_2O_3	4.39	3.74	4.51	6.42	7.32	5.24
MnO	0.05	0.04	0.03	0.02	0.03	0.05
TiO_2	0.40	0.37	0.61	0.53	0.43	0.64
CaO	6.32	5.98	7.65	3.69	3.13	8.91
Na_2O	0.01	0.04	0.69	0.01	1.06	0.69
K_2O	1.23	2.10	1.22	1.45	1.91	1.90
Total	87.87	88.14	86.41	87.13	87.53	86.47
Si/(Si+Al)	0.931	0.928	0.916	0.884	0.875	0.889
Mg/(Mg+Fe)	0.844	0.817	0.864	0.838	0.795	0.812

Results

Habit of phyllosilicates

Quartzolithic graywackes. The only authigenic clay mineral in quartzolithic graywackes is trioctahedral smectite-saponite. Saponite occurs as a pore-filling cement and usually completely occludes the intergranular spaces. Observed under the SEM, pore-filling saponite exhibits radial alignment of densely packed, up to 50 μm long platy crystals (or aggregates of crystals ?) attached approximately perpendicularly to the detrital grain surfaces. Pore-filling aggregates show well-developed medial sutures (Fig. 2A), indicating growth of crystal platelets inward from surrounding framework grains toward the center of interstitial voids (Dickinson 1970; Wilson & Pittman 1977). If seen perpendicularly to their prolongation, crystals form an irregular network with a cellular pattern (Fig. 2B). The similar boxwork-like appearance of saponite have been found in the open pores (Fig. 2C). Saponite is absent at the detrital grain contacts (Fig. 2D).

The characteristic feature of quartzolithic graywackes is scarcity of grain-alteration phyllosilicates (in contrast to the lithic graywackes described below). Only saponite infilling large pores in the vicinity of feldspar grains may be interpreted as originating by their partial replacement (Fig. 2D). Within lithic constituents, which, in these sandstones, are represented mainly by completely serpentinized ultramafic rocks, replacement textures are very rare. They can be identified in the BSE images as a zones with darker image showing shrinking cracks due to dehydration of smectitic interlayers in the vacuum chamber (Fig. 2E). Also microprobe analyses obtained from these zones indicate the presence of smectite-like layers (increased Al and Ca contents) in otherwise serpentine-dominated material. Saponite was also found in dolomite beds. It fills small cavities and displays radiating textures (Fig. 2F).

Lithic graywackes. The dominant authigenic phyllosilicate in lithic graywackes is C/S. The SEM study reveals that C/S occurs in many textural habits. The main form of occurrence, petrographically very similar to saponite, is pore-filling cement. C/S crystals are aligned radially with respect to the framework grains with distinct sutures in the center of pores (Fig. 3A). If pore space is not entirely infilled, aggregates show honeycomb patterns of curved, interlocking crystal platelets (Figs. 3B and 3C). Rarely, C/S forms flat and isomet-

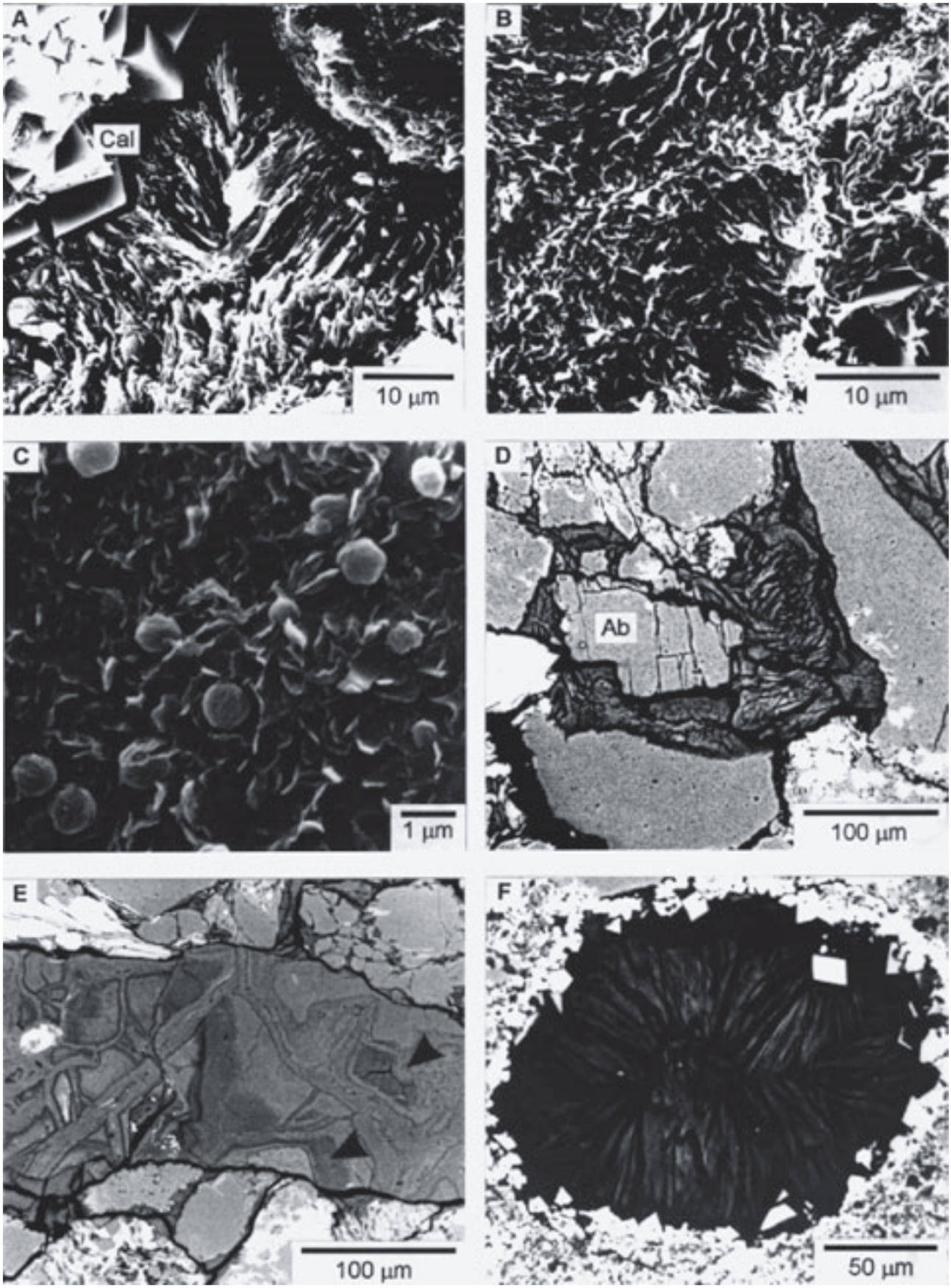
A
Cal
10 μm
B
10 μm
C
1 μm
D
Ab
100 μm
E
100 μm
F
50 μm

ric (in *ab* plane) crystals with rounded outlines, tangentially attached to the grain surface. Particles range from 1 to 3 μm in diameter and sometimes form rosette-like clusters (Fig. 3D).

The authigenic C/S also occurs as an alteration phase in lithic grains. Replacement textures are best developed within partially serpentinized detrital grains where C/S infills rounded voids after completely dissolved primary mafic mineral (olivine ?). In thin sections (BSE image), original detrital grains are recognizable through preserved mesh texture, since the serpentinized parts of clasts remained conserved (Fig. 3E). The void-filling C/S exhibit characteristic textural zonation, with coarser-grained, up to 20-μm-wide rims and fine-grained interiors. Initial parallelly stacked platelets are normal to the inner wall of voids, while later platelets display rather random arrangement (Fig. 3F). Considering the physically unstable character of clay replacements, alteration undoubtedly occurred *in situ*, as grains could not withstand transport and subsequent compaction.

In many instances lithic grains were replaced completely and their original character is unknown. However, taking into account the frequent presence of apatite and/or opaque minerals in these aggregates it is assumed that they represent altered fragments of fresh igneous minerals or vitritic clasts. Observed under the SEM, alteration C/S commonly shows multi-layered, curvilinear textures (Figs. 4A and 4B). Extensive replacement has locally resulted in almost complete destruction of the detrital framework of the sandstones. In such domains, massive aggregates of C/S commonly contain floating grains of chemically stable detrital constituents (e.g. quartz, serpentinites or large flakes of detrital phyllosilicates, Fig. 4B). On the other hand, C/S rims never occur if grain-to-grain contact is preserved.

The second diagenetic clay mineral present in lithic graywackes is saponite. Saponite is developed exclusively as a replacement phase after detrital feldspars. It usually infills small dissolution voids (Fig. 4C), but nearly complete pseudomorphs after grains were also observed (Fig. 4D). In this type of graywacke, saponite was never found as pore-filling cement. From petrographic observations, it appears that saponite replacements post-date earlier formation of C/S. Even if detrital feldspars are pseudomorphously replaced by saponite, C/S cementation is restricted to the original outlines of the grains (Fig. 4D). This textural relationship clearly reflects intense *in situ* dissolution.

Fig. 2. Photographs of authigenic saponite from quartzolithic graywackes. **A** — SEM photomicrograph of pore-filling aggregate of saponite showing radial alignment of crystallites and well-developed medial suture. Crystallites are perpendicular to the detrital grain surfaces; Cal — calcite. **B** — SEM photo of pore-filling saponite viewed perpendicularly to the prolongation of crystallites. Highly folded platelets form a cellular pattern, sometimes with a concentric organization (upper left). **C** — The boxwork-like appearance of saponite in the open pore. Saponite is overlain by opal-CT lepispheres (SEM). **D** — A large pore entirely infilled by saponite. Saponite partly replaces detrital albite grain (Ab). Surrounding framework consist of quartzose grains. Note the absence of saponite at the grain-to-grain contacts, e.g. lower right (BSE image). **E** — BSE image of detrital serpentinite grain. The darker-contrast zones are partly replaced by saponite (see text for further explanation). **F** — Saponite exhibiting radial arrangement of crystallites infills rounded cavity in metasomatically (?) dolomitized sandstones. Cavity is rimmed by euhedral crystals of Fe-dolomite (BSE image).

X-ray diffraction

Two types of authigenic layer silicates were identified by XRD study: discrete saponite and R1 ordered mixed-layered chlorite/smectite.

Saponite. XRD traces of Mg-solvated, air-dried saponite (Fig. 5A) exhibit an intense *001* reflection at about 14.6 Å, and weaker higher order *(00l)* reflections at 4.87 *(003)*, 3.65 *(004)*, 2.920 *(005)*, 2.433 *(006)* and 2.080 Å *(007)*. The basal spacing of 14.6 Å indicates two-water-interlayer complex (MacEwan & Wilson 1980). The glycerol solvation following Mg-saturation produced collapse of the saponite structure (Fig. 5A). The higher order reflections at 4.77 *(003)*, 3.58 *(004)*, 2.868 *(005)* and 2.043 Å *(007)* indicate basal spacing of approximately 14.3 Å, characteristic of single-layer glycerol complex (MacEwan & Wilson 1980). However, distinct intensity reduction and low-angle-side asymmetry of the *001* reflection suggest heterogeneity in layer charge of this clay. The estimated position of the first-order basal reflection of this additional phase at about 17 Å is indicative of two-layer glycerol complex (MacEwan & Wilson 1980). This conclusion is supported by the existence of weak reflections at 5.97 and 3.02 Å, representing *003* and *006* basal reflections, respectively (Fig. 5A — arrows). In contrast, swelling behaviour of the saponite upon Mg-saturation and ethylene glycol solvation is uniform. The XRD patterns show one series of rational *00l* reflections with *d(001)* spacings of 17.02 Å (Fig. 5A), which is indicative of two-layer glycol complex (MacEwan & Wilson 1980). In the K-saturated, air-dried samples first-order basal reflection at 12.4 Å (not shown here) suggests the presence of one-water layer hydrate (MacEwan & Wilson 1980). Heat treatment to 550 °C for one hour caused a full dehydration of this clay and collapse of the structure to 10.2 Å (Fig. 7A). XRD analysis of randomly oriented <2 μm fractions gave *06,33* reflections at 1.535 (± 0.001) Å (Fig. 5B) and a calculated unit-cell dimension of 9.21 Å. In all XRD patterns the basal reflections of saponite show a rational series of spacings, characteristic for pure mineral without structural interstratification. Clay fractions usually contain small admixtures of dioctahedral illite, chlorite and a mineral of serpentine group, which are considered to be detrital in origin.

The swelling behaviour displayed by the authigenic clay from quartzolithic graywackes is intermediate between that of smectite (i.e. two-layer glycol complex and no structural collapse upon K-saturation) and vermiculite (i.e. one-layer glycerol complex), indicating a high negative charge of the 2:1 layers. Such swelling properties are characteristic both of high-charge saponite and low-charge vermiculite, which makes categorization of this phase difficult (Malla & Douglas 1987; de la Calle & Suquet 1988). However, the layer charge of 1.05 per $O_{20}(OH)_4$ calculated from EMPA (see below) is below the limiting value of 1.20 per $O_{20}(OH)_4$, proposed by the AIPEA Nomenclature Committee for distinguishing smec-

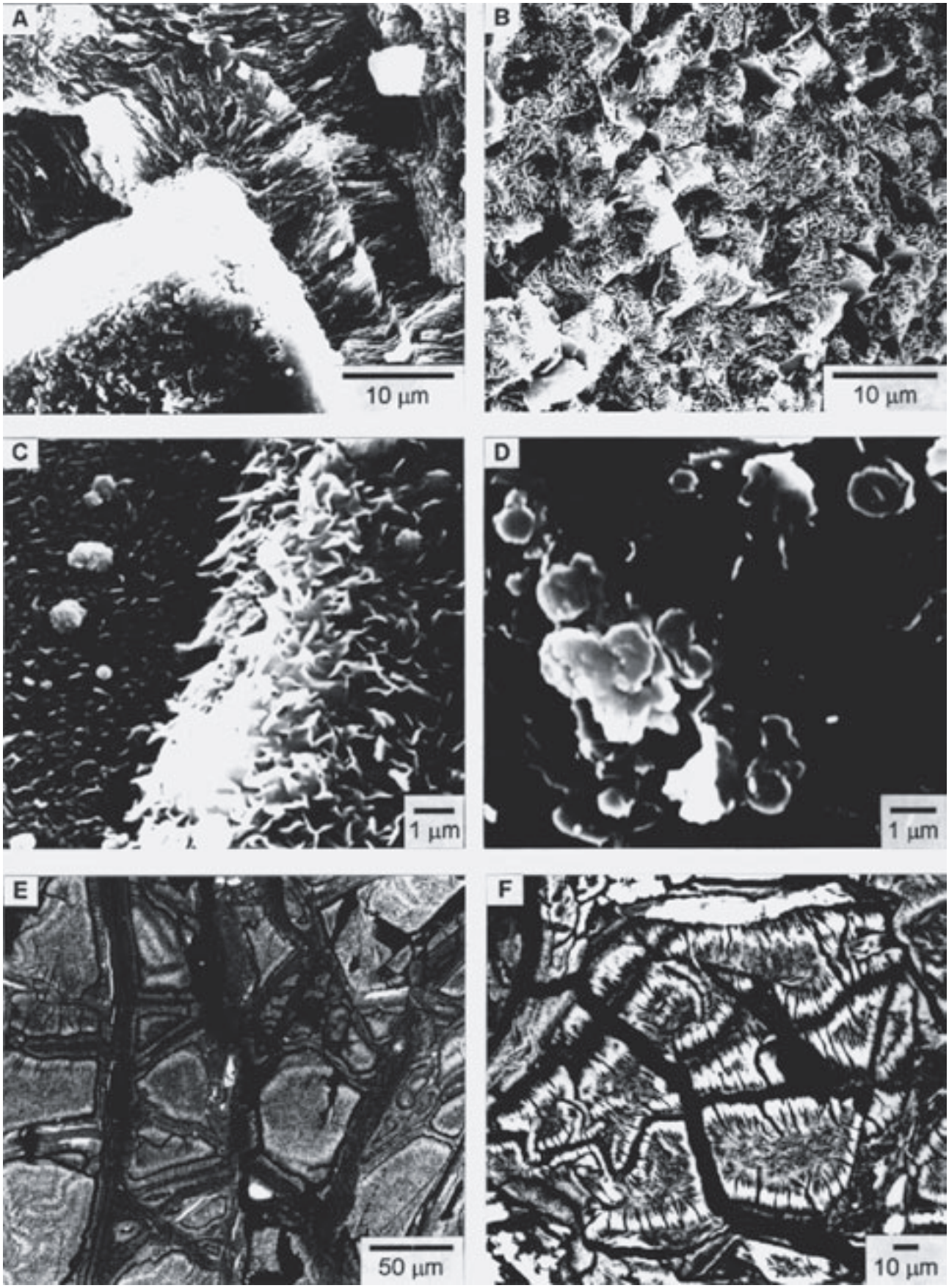
A
10 μm
B
10 μm
C
1 μm
D
1 μm
E
50 μm
F
10 μm

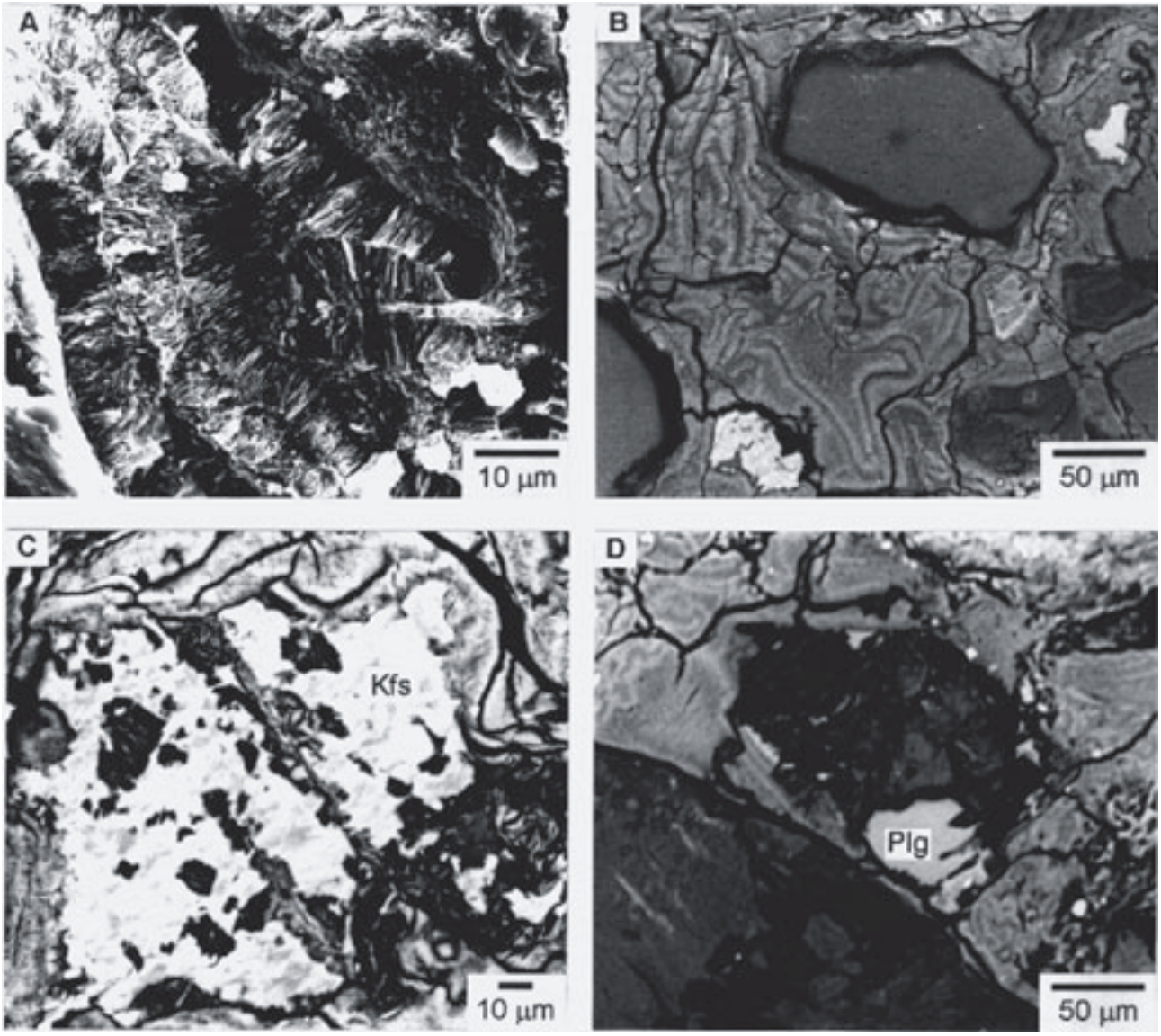

Fig. 4. Photographs illustrating C/S and saponite from lithic graywackes. **A** — SEM photo of a large pore filled by C/S showing multilayered, curvilinear texture. **B** — The same situation as in (A) seen in the BSE image. Extensive dissolution and replacement partly destroyed detrital framework of the sandstones producing massive aggregates of C/S with floating grains of chemically stable detrital constituents. **C** — BSE image of saponite filling dissolution voids in detrital grain of K-feldspar (Kfs). **D** — Detrital grain of Ca-dominated plagioclase (Plg) almost entirely replaced by saponite. Note that the formation of saponite post-dates precipitation of C/S since C/S cement respects the original outlines of detrital grains (BSE image).

Fig. 3. Photographs of diagenetic C/S from lithic graywackes. **A** — Authigenic pore-lining (or pore-filling) C/S showing growth inward from opposing sides of pores. Crystals intersect along distinct sutures near the center of the pore (SEM). **B** and **C** — Curved, interlocking crystallites of C/S organized in honeycomb arrangement (SEM). **D** — Rosette-like cluster of C/S crystallites (SEM). **E** — A detail of partly serpentinized (dark strips) detrital grain exhibiting characteristic mesh texture. Primary mafic mineral (olivine ?) was entirely replaced by C/S forming irregular-shaped aggregates with lighter contrast (BSE image). **F** — C/S filling dissolution voids in lithic grain. Note the distinct textural and compositional zonation of aggregates. The rim material consists of platy and parallelly aligned crystallites with a lighter BSE image (high Fe content) while the core material displays rather random arrangement.

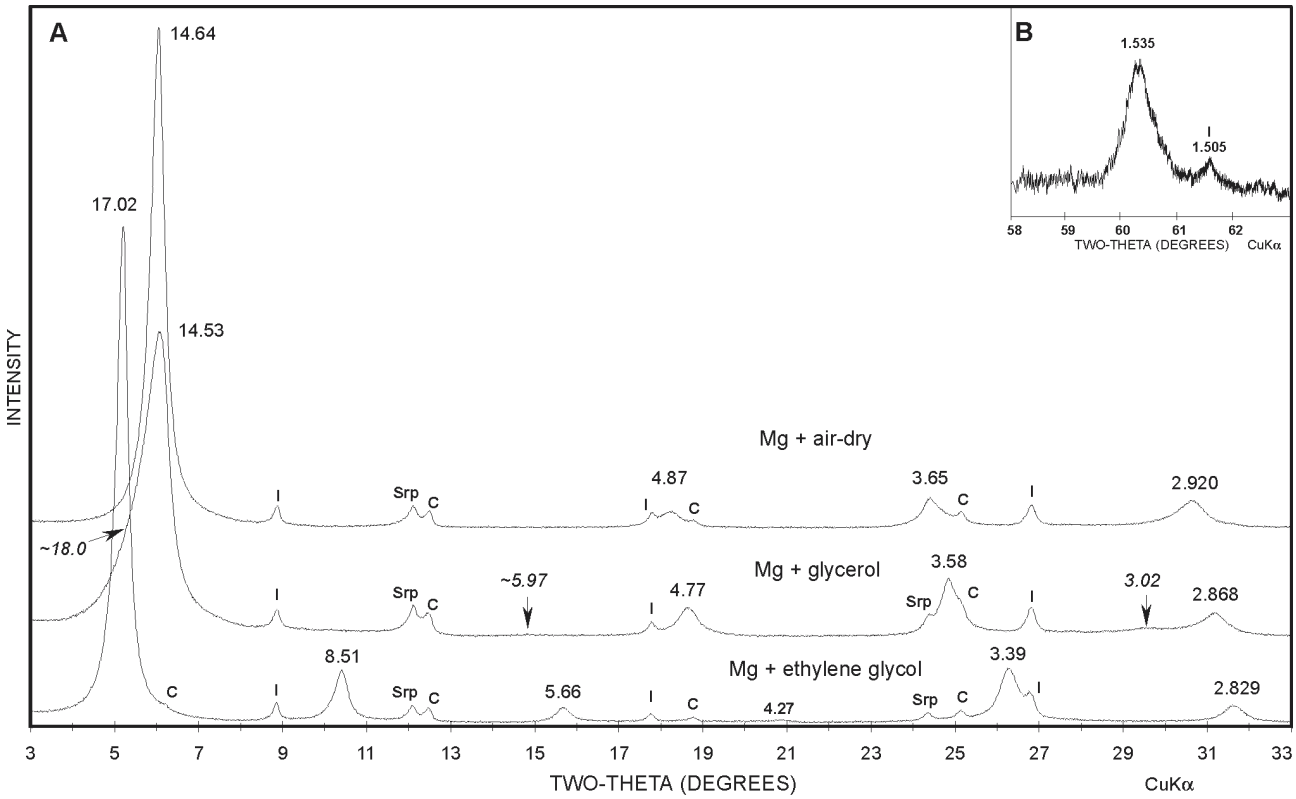

Fig. 5. A — XRD patterns of <2 μm size fractions of saponite oriented preparations in $MgCl_2$ solvated + air-dried, $MgCl_2$ + glycerol solvated, and $MgCl_2$ + ethylene glycol solvated state; **B** — *06,33* reflection of randomly oriented preparation. I — illite, Srp — serpentine, C — chlorite. *d*-spacings in Angströms.

tites from vermiculites (Bailey 1980). This defines this expandable phase as high-charge saponite. On the other hand, the ability to form simultaneously two types of glycerol complexes indicates heterogeneity in layer charge distribution (Malla & Douglas 1987; April & Keller 1992), i.e. the presence of a small proportion of a low-charge smectite.

Mixed-layer chlorite/smectite. XRD patterns of Mg-saturated, air-dried, glycerolated and glycolated mixed-layer chlorite/smectite are shown in Fig. 6. In clay fraction, C/S always occurs with discrete saponite and traces of detrital phyllosilicates (illite, chlorite, serpentine) which hampers interpretation of XRD profiles due to interference of reflections. Nevertheless, the following characteristics have been observed.

The presence of superstructure reflection near 29 Å in the air-dried pattern which shifts to 31 Å after glycolation indicates the presence of R1 ordered C/S (Reynolds 1988). Generally, these reflections as well as higher order reflections are weak and broad (particularly after ethylene glycol solvation). This suggests that the ratios of component layers in this C/S differ significantly from the ideal corrensite, and consequently, some amount of disorder. The percentage of chlorite layers was estimated on the basis of migration of basal reflections in response to ethylene glycol solvation (Reynolds 1980, 1988). Comparison of observed and calculated basal spacings indicates a chlorite content of approximately 60 %, when *004* vs. *009* (or *002/002* vs. *004/005*) peak combination is used (Fig. 6A). However, it must be noted that XRD patterns of R1 ordered mixed-layer chlorite (0.60)/smectite calculated with the NEWMOD program (Reynolds 1985; not shown here) do not fit satisfactorily with experimental XRD patterns. For example, (1) higher odd-order superstructure reflections were not observed in the Mg-saturated, air-dried patterns (particularly the *003* peak near 9.6 Å should be visible even in the presence of a small admixture of illite); (2) the *006* and *007* reflections occurring in the 16–21 °2Θ CuKα range after ethylene glycol solvation are not resolved. Hillier (1995) showed that any R1 chlorite/smectite always has a mixed-layer (R0) chlorite/corrensite equivalent. Using a partially segregated arrangement of component layers, he was able to simulate an XRD pattern which still has a peak at 31 Å (EG) but other diffraction maxima are broad and shifted. On the basis of these findings, Hillier (1995) concluded that the shoulder at 31 Å is not related to any kind of ordering but rather to the presence of a 31 Å component layer (i.e. corrensite). This might suggest that crystallites with partially segregated packets of corrensite and chlorite layers are also present in chloritic material from lithic graywackes, which could be consistent with textural heterogeneity observed in the SEM study. However, no attempt was made to simulate such a type of structure.

The swelling properties of C/S are very similar to those previously described for the saponite. Mg-saturated, air-dried C/S shows basal reflections at ~29.4, 14.54, 7.26, 4.82, 3.60, 2.893 and 2.057 Å (Fig. 6A). Upon glycerol solvation of this same sample, a structural contraction occurred, as indicated

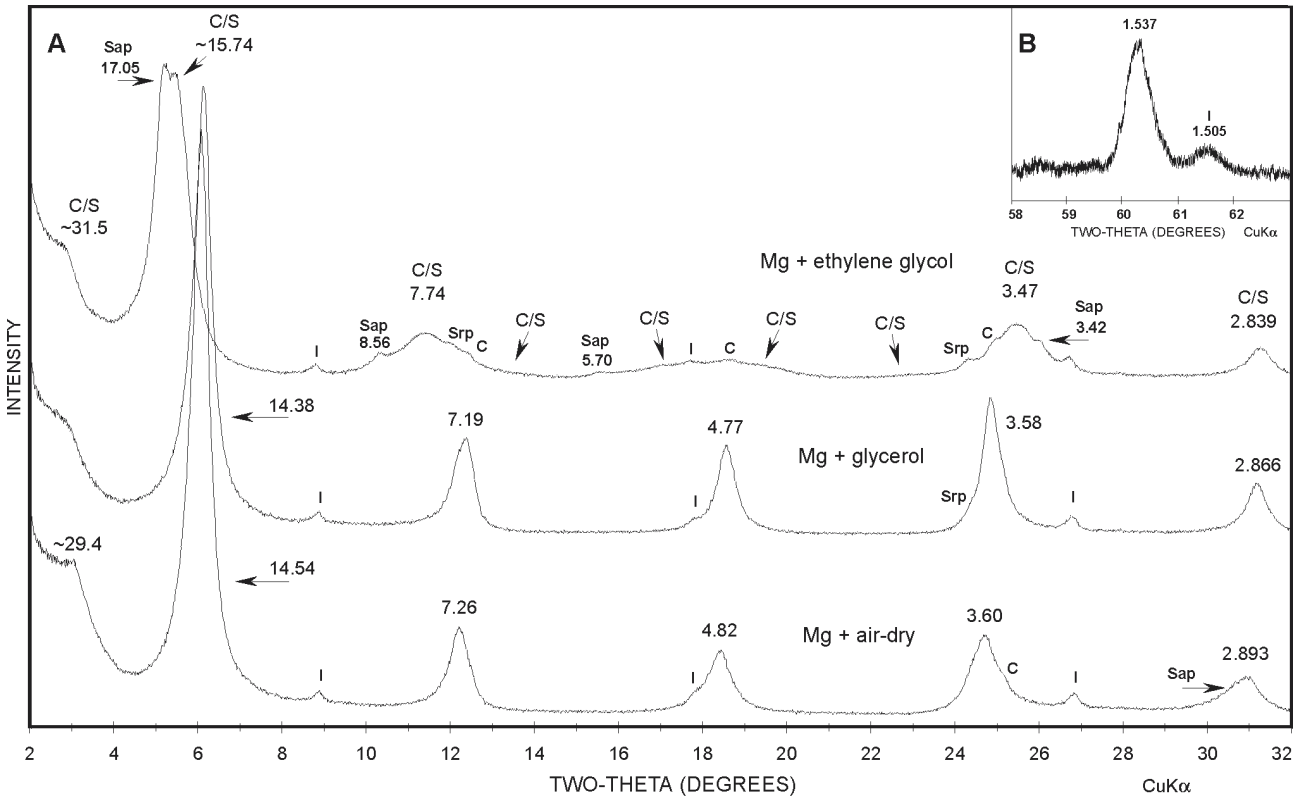

Fig. 6. A — XRD patterns of <2 μm size fractions of mixed-layer chlorite/smectite (C/S) oriented preparations in $MgCl_2$ solvated + air-dried, $MgCl_2$ + glycerol solvated, and $MgCl_2$ + ethylene glycol solvated state; **B** — XRD pattern of *06,33* reflection of randomly oriented preparation. Sap — saponite, I — illite, Srp — serpentine, C — chlorite. *d*-spacings in Angströms.

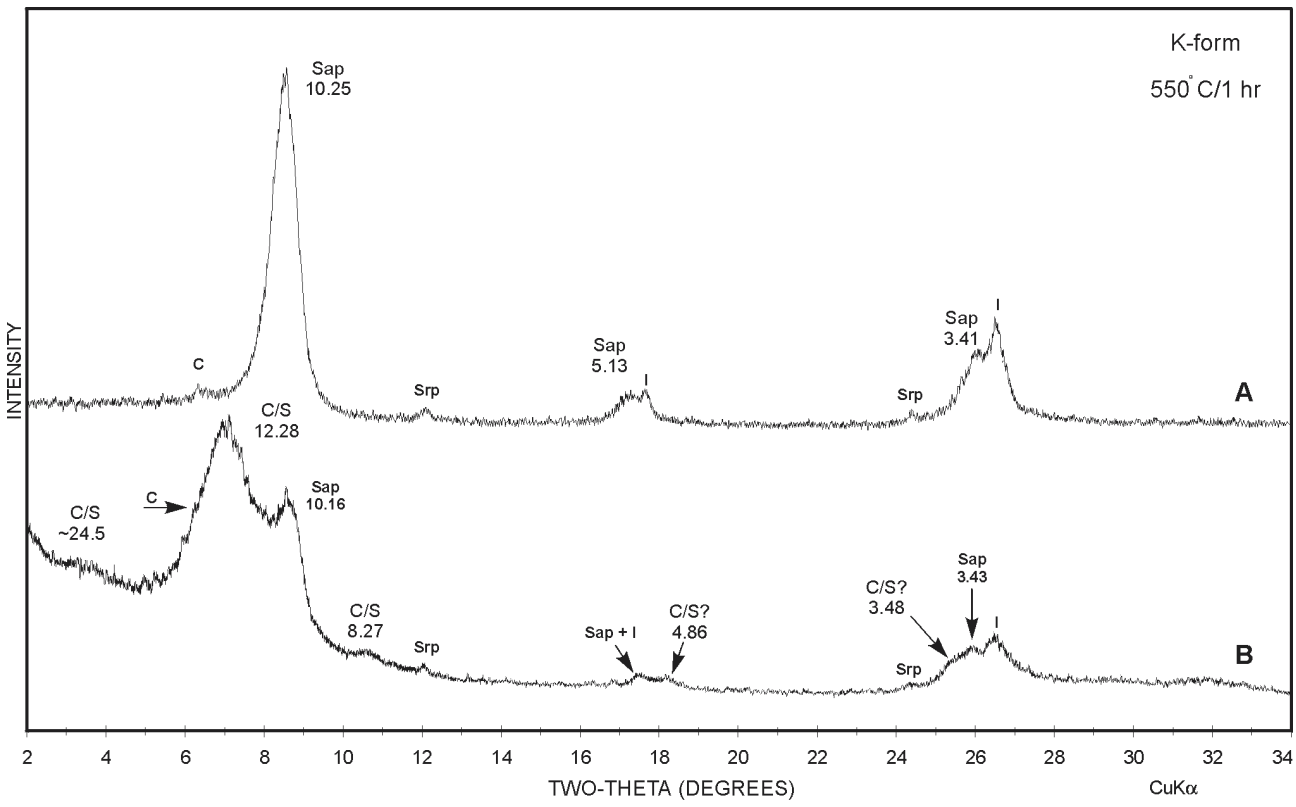

Fig. 7. XRD patterns of <2 μm size fractions of (**A**) saponite and (**B**) mixed-layer chlorite/smectite after K-saturation and heating to 550 °C for 1 hr. C/S — mixed-layer chlorite/smectite, Sap — saponite, I — illite, Srp — serpentine, C — chlorite. *d*-spacings in Angströms.

by the shift of reflections towards the higher degrees two-theta (Fig. 6A). With ethylene glycol solvation Mg-saturated C/S expands to ~31.5 Å. Glycol solvation also produces resolution of overlapping peaks. Similarly, heat treatment of K-saturated samples at 550 °C for one hour resulted in two series of reflections with *001* spacings of ~25 and ~10.2 Å, respectively, the former representing collapsed C/S and the latter collapsed saponite (Fig. 7B). This means, that charge of expandable interlayers must be high enough to produces both vermiculite-like and smectite-like swelling behaviour. By analogy with the above described expansion properties of discrete saponite, the expandable component of this mixed-layer mineral can be tentatively categorized as high-charge saponite.

Randomly orientated C/S-rich clay fractions display strong *06,33* reflection at 1.537 (±0.001) Å (Fig. 6B). However, this value cannot be safely attributed to C/S because of substantial admixture of saponite and probable peak interference.

Electron microprobe data

Authigenic phyllosilicates examined in this study, occur in exceptionally well developed and densely packed aggregates (pore-fillings, pseudomorphic replacements within lithic grains). Therefore, microprobe analyses can be used to determine their compositional characteristics with reasonable confidence. The following discussion assumes that total Fe is in the Fe^{2+} state.

Saponite. Representative chemical analyses of saponite are given in Table 2. The structural formulae have 6.15–6.31 octahedral cations (i.e. Al^{VI} + Mg + Fe + Mn), which is considerably higher than the theoretical trioctahedral limit of 6 cations per $O_{20}(OH)_4$. The high octahedral occupancy indicates, that the smectite is either structurally interstratified with a small percentage of chlorite component or intergrown with another chloritic mineral. Considering the XRD data, a mixed-layering can be eliminated (see *X-ray diffraction* section). The existence of intimate intergrowths with chloritic phase is difficult to detect, however, contamination of EMPA should result in a positive correlation between total Al contents and octahedral cation totals, which is not the case (r = 0.09; see also Fig. 9B). The second possible interpretation is that the saponite contains a small amount of Mg ions located in the interlayer position. This alternative was recently verified by Beaufort & Meunier (1994) as well as Schiffman & Southard (1996) for saponites from metabasaltic rocks. Saponite from serpentinitic graywackes have formed in environments exceptionally rich in Mg (see Table 1), therefore, the presence of the interlayer Mg is also highly probable. Moreover, assignment of the „excess“ Mg (~0.20 cations/$O_{20}(OH)_4$) to the exchangeable sites presented in Table 2 increases the interlayer charge of the saponite. This approach seems reasonable as the prevalence of high-charge layers was deduced from the XRD results.

The saponites from the quartzolithic graywackes exhibit only negligible compositional variations between samples.

Table 2: Representative electron microprobe analyses of saponite.

Sample	258/V	258/V	258/V	K-I	K-I	K-I	255/II	255/II	255/II	256/TM1
Oxygen basis					$O_{20}(OH)_4$					
Habit	pore	pore	pore	pore	pore	pore	pore	pore	pore	Plg-replace
SiO_2	45.02	42.87	41.47	47.15	46.38	44.57	46.61	44.25	44.00	45.11
Al_2O_3	5.80	5.79	5.65	6.48	6.17	5.73	6.19	5.78	5.88	6.57
MgO	25.09	23.41	23.39	24.95	23.60	23.71	24.81	23.01	23.94	23.36
FeO[1]	2.86	3.31	2.30	4.49	4.28	4.06	4.32	3.82	4.49	5.48
MnO	0.07	0.08	0.02	0.00	0.00	0.00	0.00	0.00	0.00	0.00
CaO	2.12	2.51	1.48	1.66	1.79	1.80	1.36	1.49	1.68	1.88
Na_2O	0.06	0.05	0.04	0.03	0.00	0.05	0.06	0.00	0.04	0.05
K_2O	0.00	0.00	0.00	0.03	0.08	0.00	0.01	0.06	0.02	0.00
Total	81.02	78.02	74.35	84.79	82.30	79.92	83.36	78.41	80.05	82.45
Si	6.948	6.911	6.945	6.976	7.066	7.004	7.008	7.062	6.930	6.925
Al(IV)	1.053	1.089	1.055	1.024	0.934	0.996	0.992	0.938	1.070	1.075
SumIV	8.000	8.000	8.000	8.000	8.000	8.000	8.000	8.000	8.000	8.000
Al(VI)	0.002	0.011	0.060	0.107	0.174	0.065	0.104	0.149	0.021	0.114
Mg(VI)	5.620	5.529	5.615	5.340	5.281	5.400	5.348	5.341	5.388	5.183
Fe	0.369	0.446	0.322	0.556	0.545	0.534	0.543	0.510	0.591	0.704
Mn	0.009	0.011	0.003	0.000	0.000	0.000	0.000	0.000	0.000	0.000
SumVI	6.000	6.000	6.000	6.000	6.000	6.000	6.000	6.000	6.000	6.000
Mg(IL)[2]	0.150	0.097	0.225	0.160	0.080	0.154	0.213	0.134	0.233	0.164
Ca	0.351	0.434	0.266	0.263	0.292	0.303	0.219	0.255	0.284	0.309
Na	0.018	0.016	0.013	0.009	0.000	0.015	0.018	0.000	0.012	0.015
K	0.000	0.000	0.000	0.006	0.016	0.000	0.002	0.012	0.004	0.000
SumIL	0.519	0.546	0.504	0.438	0.388	0.472	0.451	0.401	0.533	0.488
ILC[3]	1.020	1.076	0.994	0.860	0.760	0.929	0.883	0.789	1.049	0.961
Si/(Si+Al)	0.868	0.863	0.862	0.861	0.864	0.868	0.865	0.867	0.864	0.853
Mg/(Mg+Fe)	0.940	0.927	0.948	0.908	0.908	0.912	0.911	0.915	0.905	0.884

NOTE: [1] total Fe as FeO, [2] calculated from stoichiometry, [3] interlayer charge including Mg(IL)

Table 3: Selected electron microprobe analyses of mixed-layer chlorite/smectite.

Sample	256/TM1									
Oxygen basis	$O_{20}(OH)_{10}$									
Habit	pore	pore	pore	pore	replace	replace	replace	replace	replace	replace
	core	core	core	core	core	core	core	rim	rim	rim
SiO_2	38.77	39.60	39.14	38.80	38.85	36.78	39.91	36.53	36.81	37.55
Al_2O_3	13.33	13.69	13.40	13.09	13.59	14.49	13.36	15.50	17.00	16.54
MgO	27.49	26.85	28.12	26.94	26.82	25.67	26.74	21.82	22.02	23.91
FeO[1]	8.97	9.18	9.09	8.81	9.60	9.51	8.92	11.97	12.22	10.90
MnO	0.25	0.09	0.00	0.11	0.00	0.15	0.00	0.00	0.00	0.16
CaO	0.68	0.64	0.70	0.82	0.62	0.97	0.58	0.50	0.36	0.73
Na_2O	0.00	0.00	0.13	0.01	0.06	0.08	0.04	0.14	0.00	0.09
K_2O	0.00	0.00	0.00	0.00	0.00	0.03	0.00	0.01	0.03	0.00
Total	89.49	90.05	90.58	88.58	89.54	87.68	89.56	86.60	88.44	89.88
Si	6.439	6.519	6.422	6.499	6.455	6.270	6.589	6.349	6.255	6.254
Al(IV)	1.561	1.481	1.578	1.501	1.545	1.730	1.411	1.651	1.745	1.746
Sum IV	8.000	8.000	8.000	8.000	8.000	8.000	8.000	8.000	8.000	8.000
Al(VI)	1.048	1.175	1.013	1.083	1.117	1.181	1.188	1.525	1.660	1.501
Mg(VI)	6.671	6.549	6.740	6.667	6.549	6.442	6.579	5.654	5.578	5.937
Fe	1.246	1.264	1.247	1.234	1.334	1.356	1.232	1.740	1.737	1.518
Mn	0.035	0.013	0.000	0.016	0.000	0.022	0.000	0.000	0.000	0.023
Sum VI	9.000	9.000	9.000	9.000	9.000	9.000	9.000	8.930	8.974	8.978
Mg(IL)[2]	0.135	0.040	0.139	0.060	0.094	0.081	0.002	0.000	0.000	0.000
Ca	0.121	0.113	0.123	0.147	0.110	0.177	0.103	0.093	0.066	0.130
Na	0.000	0.000	0.041	0.003	0.019	0.026	0.013	0.047	0.000	0.029
K	0.000	0.000	0.000	0.000	0.000	0.007	0.000	0.002	0.007	0.000
Sum IL	0.256	0.153	0.303	0.210	0.224	0.291	0.117	0.143	0.072	0.159
Si/(Si+Al)	0.712	0.711	0.713	0.716	0.708	0.683	0.717	0.648	0.648	0.658
Mg/(Mg+Fe)	0.845	0.839	0.846	0.845	0.833	0.828	0.842	0.763	0.763	0.796

NOTE: [1] total Fe as FeO; [2] calculated from stoichiometry

The Si/(Si + Al) ratio is almost uniform, ranging from 0.85 to 0.87, while the total Mg/(Mg + Fe) ratio varies from 0.89 to 0.95 (Table 2). The average Al^{VI} content ranges from 0.04 to 0.11 cations per $O_{20}(OH)_4$, which is in agreement with the essentially trioctahedral character of these smectites indicated by XRD data. Sample 256/TM1 represents saponite 'coexisting' with the C/S in lithic graywackes. Its Mg/(Mg + Fe) ratio of 0.88 is the lowest found in this study (Table 2).

The sum of interlayer cations (i.e. calculated MgIL + Ca + Na + K) ranges between 0.35 and 0.55 cations/$O_{20}(OH)_4$. In addition to the only presumed interlayer Mg, Ca is the most abundant interlayer cation with very minor to negligible amounts of Na and K (Table 2). Taking into account the exchangeable Mg, saponite shows a large variation of interlayer charge ranging from 0.69 to 1.08/$O_{20}(OH)_4$, with mode of 1.05/$O_{20}(OH)_4$. A large interval may reflect a heterogeneity in layer charge distribution also inferred from the swelling properties of this phase. The layer charge is derived solely from tetrahedral substitution of Al for Si.

Mixed-layer chlorite/smectite. The C/S-rich sample 256/TM1 was investigated in detail. Results of 42 spot analyses normalized on the $O_{20}(OH)_{10}$ basis (i.e. corrensite formula) are presented as a series of histograms in Fig. 8. In addition, selected analyses are shown in Table 3. In contrast to the XRD data, composition of this phase suits the composition of ideal corrensite fairly well. The number of cations in the octahedral sites is between 8.70 and 9.18 per $O_{20}(OH)_{10}$ (with mode 8.93/$O_{20}(OH)_{10}$), which is consistent with combination of one chlorite-like layer (6 octahedral cations per $O_{10}(OH)_8$) and one saponite-like layer (3 octahedral cations per $O_{10}(OH)_2$). However, BSE imaging revealed textural as well as chemical zoning of C/S aggregates. The compositional heterogeneity is also confirmed by the EMPA data. Two compositions were detected in sample 256/TM1, as evident from the bimodal distribution of major elements in the histograms (Fig. 8). The first set of analyses was obtained from fine-grained phyllosilicates occurring in the central parts of pore-fillings as well as aggregates replacing detrital grains. The second group of analyses represents platy and prolonged crystallites, which form thin rims around the core material (Figs. 3F and 4B). The composition of core C/S differs from the composition of rim C/S by having a higher Si/(Si + Al) ratio (0.72 vs. 0.68) and a higher Mg/(Mg + Fe) ratio (0.84 vs. 0.80; see also Fig. 9 — open squares vs. filled squares and Table 3). The opposite trend was observed by Shau et al. (1990) in chloritic minerals in amygdaloidal metabasalts from the northern Taiwan. Using EMPA and TEM/AEM data, they observed that textural and chemical zonation of aggregates also indicates structural changes in phyllosilicates. They concluded that increase in total Al content and decrease in Mg/(Mg + Fe) ratio and Ca content from rim to core of amygdales correlate with the increasing chlorite component in the mixed-layered chlorite/smectite (or mixed-layered chlorite/corrensite). This may suggest the similar in-

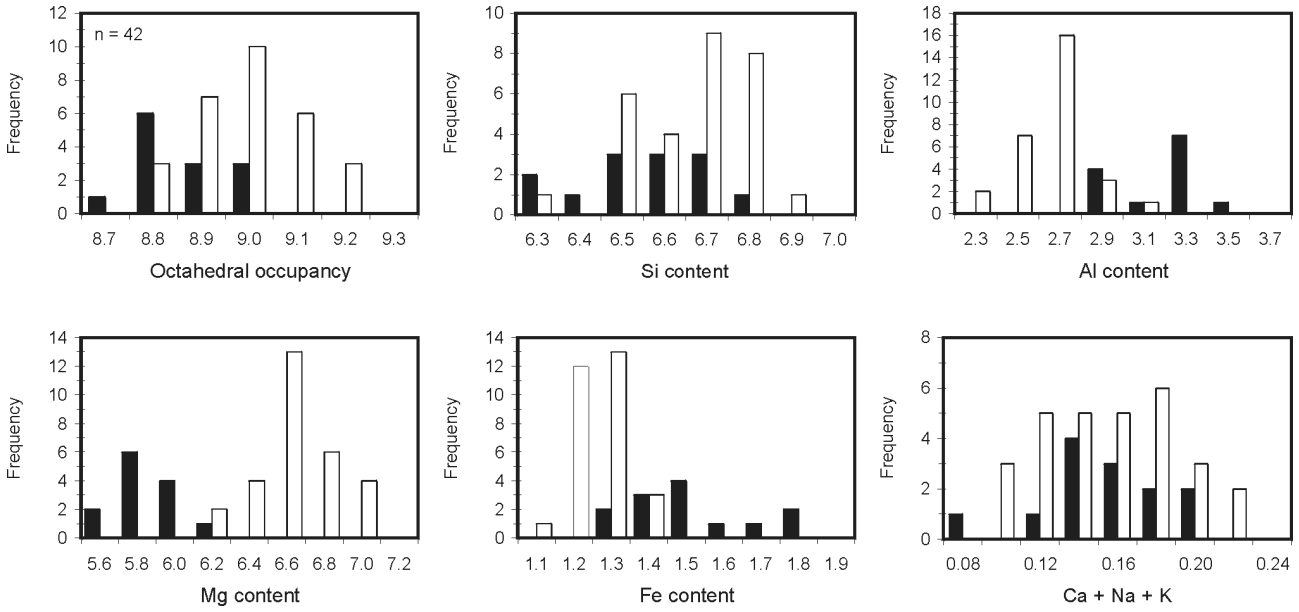

Fig. 8. Results of microprobe analyses of zoned C/S (sample 256/TM1) presented as histograms. Normalization on the basis of $O_{20}(OH)_{10}$. *Open columns* — core material, *filled columns* — rim material.

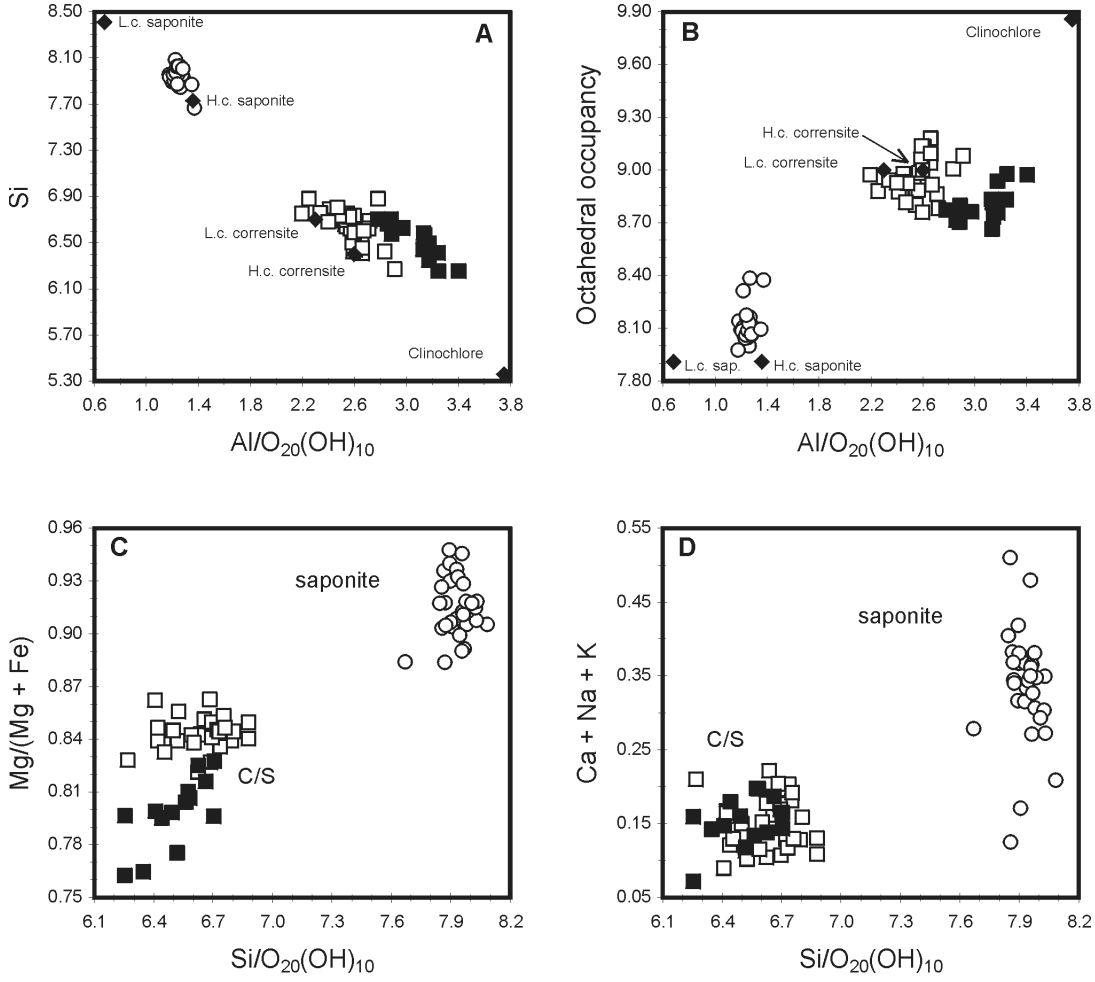

Fig. 9. Composition of diagenetic phyllosilicates from the serpentinitic graywackes obtained from microprobe analyses: (**A**) Si vs. Al, (**B**) octahedral occupancy vs. Al, (**C**) Mg/(Mg+Fe) vs. Si, (**D**) Ca+Na+K vs. Si. All recalculated on the $O_{20}(OH)_{10}$ basis; total iron as Fe^{2+}. The compositions of ideal low-charge (L.c.) and high-charge (H.c.) saponite and corrensite, as well as the composition of clinochlore, are given for reference (*filled diamonds*). *Open circles* — saponite; *open squares* — core C/S, *filled squares* — rim C/S.

crease of the chlorite component in the rim material found in lithic graywackes. Fig. 9A shows that the analysis points of rim C/S are truly shifted towards the chlorite composition. In addition, Beaufort et al. (1997) observed that the honeycomb morphology of C/S diminishes and the resolution of individual crystals increase as these phases become more chloritic (see also Wilson & Pittman 1977). Thus, a distinct platy habitat of rim crystals may be regarded as a further (but indirect) evidence in favour of this interpretation. On the other hand, the rim C/S has octahedral occupancy comparable with core C/S, ranging from 8.70 to 8.98/$O_{20}(OH)_{10}$ (see also Figs. 8 and 9B). Furthermore, both types of phyllosilicates show approximately equal (average) sums of interlayer cations (i.e. Ca + Na + K = 0.153 vs. 0.150/$O_{20}(OH)_{10}$; Fig. 9D). Considering all these facts, we are not able to identify with certainty the real physical nature of the rim material. However, the possible coexistence of chlorite-dominated phase along with corrensite may explain the poorly defined XRD traces observed in this study (Hillier 1995; Beaufort et al. 1997).

Compositional relationships between phyllosilicates. The diagrams shown in Fig. 9 illustrate basic compositional distinctions between the studied phyllosilicates. To facilitate this comparison, both saponite and C/S analyses were normalized on the basis of the corrensite formula (i.e. 25 oxygens). In general, the total Al content increases and the Si content decreases from saponite to C/S, without compositional overlap (Fig. 9A). The saponite exhibits a higher total Mg/(Mg + Fe) ratio (Fig. 9C) as well as higher content of interlayer cations than C/S (Fig. 9D). In addition, Figs. 9A and 9B clearly illustrate that the C/S (particularly core material) observed in lithic graywackes is compositionally very close to a 50:50 mixture of chlorite and trioctahedral smectite. The observed compositional trend of increasing Al content and decreasing Mg/(Mg + Fe) in the order of saponite to C/S is consistent with compositional relations between these minerals in basalt alteration parageneses (Shau et al. 1990; Shau & Peacor 1992).

Discussion

Origin of the phyllosilicate cement

In the graywackes from the Šambron Zone, clay minerals are clearly authigenic. There is no evidence, such as coatings composed of clay platelets oriented tangentially to grain surfaces, fluid internal fabric and polymineralic composition of aggregates or presence of fine-grained impurities, that the phyllosilicates may have been formed by diagenetic recrystallization of a pre-existing (syndepositional or mechanically infiltrated) detrital clay matrix (Dickinson 1970; Wilson & Pittman 1977; Moraes & Ros 1992). On the contrary, several facts lead us to suggest that both saponite and C/S originated by the interaction of the sediment with pore-fluids during burial as a direct precipitates: (1) perpendicular alignment of crystallites to detrital grain boundaries, indicating growth in open pores; (2) the delicate habit of crystallites in the preserved open pore spaces; (3) the chemical and structural (?) zonation of C/S aggregates, most probably reflecting a temporal and spatial evolution of the pore-fluid chemistry (Shau et al. 1990; Shau & Peacor 1992; Bautier et al. 1995); (4) the monomineralic, either saponitic or corrensitic, composition of the clay cement; and (5) *in situ* dissolution and replacement of lithic fragments.

In the case of C/S, however, another feasible model of its origin should be considered — diagenetic alteration of an earlier saponite precursor. Such a prograde conversion of trioctahedral smectite to chlorite through the ordered interstratified chlorite/smectite (corrensite) during burial diagenesis has been recorded by a number of authors from various geological environments (see *Introduction* section). The process seems to be strongly temperature dependent, but little is known about the mechanisms governing the reaction pathways. A simple progressive interstratification of the brucitic interlayers in the original saponite (i.e., solid-state transformation), proposed by Bodine & Madsen (1987), is unlikely. A large compositional gap between saponite and C/S observed in this study (Fig. 9) indicates that the 2:1 layers in these two phases have completely different chemical composition. It means, that the structure and chemistry of the 2:1 layers in C/S could not be inherited from the crystalline structure of the original smectite. Therefore, the crystallization of C/S at the expense of saponite would require a dissolution/precipitation mechanism, as proposed by Meunier et al. (1991). The presence of saponite in the C/S-rich graywackes supports this idea. However, petrographic evidence shows that in this type of graywackes saponite postdates the formation of C/S and from some reason it occurs only as a replacing phase within the detrital feldspars. Furthermore, the dissolution/precipitation mechanism should result in modification of early diagenetic textures of clay cement, which is not the case (see above). Considering these facts, a direct precipitation of C/S from solution is suspected rather than the smectite-to-corrensite conversion.

Factors controlling precipitation of phyllosilicates

The development of trioctahedral Mg-rich clay minerals is undoubtedly related to abundant lithic material in the sandstones. Its gradual chemical dissolution may have released plentiful supplies of Si, Al, Mg and Fe into the solution, so that the activities of the required ions in porewaters were sufficiently high for direct precipitation of clay minerals. Evidence for this includes the large quantities of alteration textures and local metasomatic (?) dolomitization of sandstones. However, the important question is: "Why do sandstones located within one small outcrop have either saponitic or corrensitic cementation". It is obvious that both types of sandstones underwent the same burial history therefore the temperature factor can be neglected. As described earlier, however, there are significant differences in the modal composition of the host sandstones (Table 1). This suggests that a different bulk rock composition, and consequently, a different chemistry of pore-fluids played an important role during authigenesis, being favourable either for saponite or C/S stability. As can be seen in Fig. 10, there is a very strong positive correlation (r = 0.96) between phyllosilicate Si/(Si + Al) ratios and corresponding whole-rock values. It indicates, that Al-rich C/S has formed only in the graywackes with suffi-

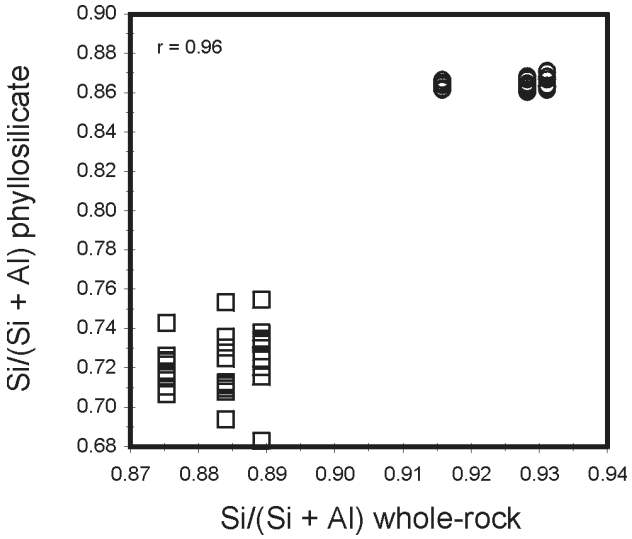

Fig. 10. Plot of phyllosilicate Si/(Si + Al) vs. whole-rock Si/(Si + Al), demonstrating a strong positive correlation (r = 0.96) between these two variables. Structural formulae calculated on the $O_{20}(OH)_{10}$ basis. *Circles* — saponite : quartzolithic graywackes; *squares* — C/S : lithic graywackes.

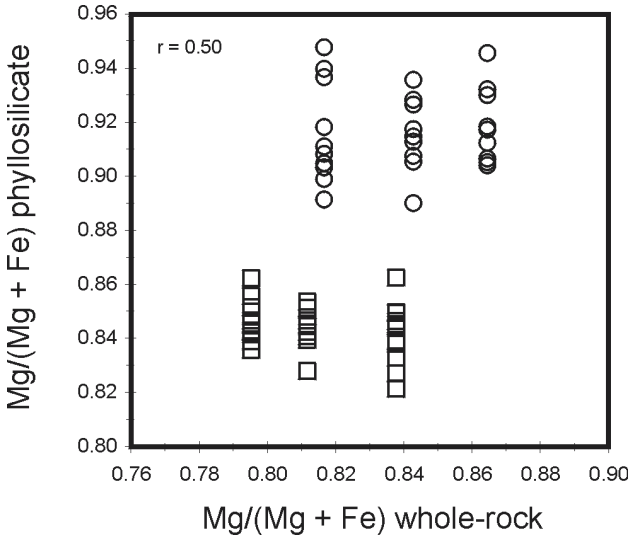

Fig. 11. Mg/(Mg + Fe) ratios of phyllosilicates plotted against corresponding whole-rock values. Note the weak correlation between these two variables. Structural formulae calculated on the $O_{20}(OH)_{10}$ basis. *Circles* — saponite : quartzolithic graywackes; *squares* — C/S : lithic graywackes.

cient Al contents. In other words, the amount of available Al may have been a primary factor in controlling the precipitation of phyllosilicates. The importance of the whole-rock Al content for the formation of the trioctahedral phyllosilicates in Mg-rich environments has been pointed out by Shau & Peacor (1992), Hillier (1993) and Beaufort & Meunier (1994). Experimental studies by Velde (1977) also imply that the occurrence of the regularly interstratified (R1) phase instead of smectite or chlorite may be controlled by the amount of R^{3+} component in the system (the Al^{3+} or Fe^{3+} content of the assemblage). However, it should be noted that different availability of Al cannot be simply attributed to the percentage of lithic grains in the individual sandstone beds because they are mostly represented by the Al-poor serpentinites. Assuming low mobility of Al-ions during diagenesis (Wintsch & Kvale 1994), there must have been an other potential source of Al, which was present in some sandstones at the time of deposition. The role of feldspars is not considered here, due to their accessory amounts in sediments. In addition, textural relationships suggest that the main phase of feldspar dissolution post-dates formation of the pore-filling phyllosilicates. However, the graywackes, in which C/S dominates, are characterized by large domains with an extensively altered detrital framework. It has been proposed that they mostly represent replaced glassy fragments or mafic minerals. As the equivalent replacement textures have not been observed in the quartzolithic graywackes (with saponitic cementation), it is possible to suggest that presence or absence of these highly unstable detrital components in original sediments was crucial for their diagenetic evolution.

Several authors have also discussed an influence of bulk-rock or fluid Mg/(Mg + Fe) ratio on the occurrence of smectite, corrensite or chlorite (Almon et al. 1976; Velde 1977; Brigatti & Poppi 1984; Shau et al. 1990). Results obtained from different geological and rock environments infer that saponite is favoured by a high bulk-rock or fluid Mg/(Mg + Fe) ratio whereas corrensite (or chlorite) is favoured to form in rocks with a lower Mg/(Mg + Fe) ratio (Brigatti & Poppi 1984). The data presented here do not show such relationship. In fact, differences in whole-rock Mg/(Mg + Fe) values between saponite- and C/S-rich graywackes are negligible, ranging from 0.817 to 0.864, and 0.795 to 0.838, respectively (Table 1). Furthermore, as shown in Fig. 11, there is only weak correlation between phyllosilicate and whole-rock Mg/(Mg + Fe) ratios. This implies that the composition of saponite and C/S with respect to Mg/(Mg + Fe) ratio is unique and independent of whole-rock chemistry. Shau et al. (1990) have proposed that the contents of Fe (relative to Mg) and Al^{IV} (relative to Si) increase in the order of saponite, corrensite, to chlorite as a consequence of minimization of the misfit between octahedral and tetrahedral sheets within the 2 : 1 layers (i.e. due to unique crystal-chemical relations in each mineral). The substitution of Al^{IV} for Si causes an increase in size of the tetrahedral sheets, which requires a substitution of the larger Fe^{2+} ions for Mg^{2+} in the octahedral sheets in order to compensate for such changes. Our results seem to offer further evidence in favour of this idea.

Acknowledgements: The authors are grateful to Ľubica Puškelová (Geological Institute of Slovak Academy of Sciences) for XRF and XRD analyses. We also wish to express special thanks to Pavol Siman and his staff at the Geological Survey of Slovak Republic for their technical assistance in the SEM/EMPA work. Financial support for this study was provided by the Scientific Grant Agency (VEGA), grants No. 2/4077/97 and No. 95/5305/520.

References

Almon W.R., Fullerton L.B. & Davies D.K., 1976: Pore space reduction in Cretaceous sandstones through chemical precipitation of clay minerals. *J. Sed. Petrology*, 46, 89–96.

April R.H., 1981: Trioctahedral smectite and interstratified chlorite/smectite in Jurassic strata of the Connecticut Valley. *Clays and Clay Miner.*, 29, 31–39.

April R.H. & Keller D.M., 1992: Saponite and vermiculite in amygdales of the Granby basaltic tuff, Connecticut Valley. *Clays and Clay Miner.*, 40, 22–31.

Bailey S.W., 1980: Summary of recommendations of AIPEA nomenclature committee. *Clays and Clay Miner.*, 28, 73–78.

Bautier M.D., Früh-Green G.L. & Karpoff A.M., 1995: Mechanism of Mg-phyllosilicate formation in a hydrothermal system at a sedimented ridge (Middle Valley, Juan de Fuca). *Contr. Mineral. Petrology*, 122, 134–151.

Beaufort D. & Meunier A., 1994: Saponite, corrensite and chlorite-saponite mixed-layer in the Sancerre-Couy deep drill-hole (France). *Clay Miner.*, 29, 47–61.

Beaufort D., Baronnet A., Lanson B. & Meunier A., 1997: Corrensite: A single phase or a mixed-layer phyllosilicate in the saponite-to-chlorite conversion series? A case study of Sancerre-Couy deep drill hole (France). *Amer. Mineralogist*, 82, 109–124.

Bettison L.A. & Schiffman P., 1988: Compositional and structural variations of phyllosilicates from the Point Sal ophiolite, California. *Amer. Mineralogist*, 73, 62–76.

Bettison-Varga L.A., MacKinnon I.D.R. & Schiffman P., 1991: Integrated TEM, XRD, and electron microprobe investigation of mixed-layer chlorite/smectite from the Point Sal ophiolite, California. *J. Metamorphic Geol.*, 9, 697–710.

Bodine M.W. & Madsen B.M., 1987: Mixed-layer chlorite/smectites from a Pennsylvanian evaporite cycle, Grand County, Utah. *Proc. Int. Clay Confer. 1985, Denver.*, *Clay Miner. Soc.,* Bloomington, Indiana, 85–96.

Brigatti M.F. & Poppi L., 1984: Crystal chemistry of corrensite: a review. *Clays and Clay Miner.*, 32, 391–399.

Chang H.K., Mackenzie F.T. & Schoonmaker J., 1986: Comparisons between the diagenesis of dioctahedral and trioctahedral smectite, Brazilian offshore basins. *Clays and Clay Miner.*, 34, 407–423.

De la Calle C. & Suquet H., 1988: Vermiculite. In: Bailey S.W. (Ed.): *Hydrous Phyllosilicates (exclusive of micas). Rev. in Mineralogy, Vol. 19, Mineral. Soc. Amer.,* 455–496.

Dickinson W.R., 1970: Interpreting detrital modes of graywacke and arkose. *J. Sed. Petrology*, 40, 659–707.

Fisher R.S., 1988: Clay minerals in evaporite host rocks, Palo Duro Basin, Texas Panhandle, *J. Sed. Petrology*, 58, 836–844.

Füchtbauer H., 1959: Zur Nomenklatur der Sedimentgesteine. *Erdöl u. Kohle*, 12, 605–613.

Galloway W.E., 1974: Deposition and diagenetic alteration of sandstone in northwest Pacific arc-related basins: Implications for graywacke genesis. *Geol. Soc. Amer. Bull.*, 85, 379–390.

Helmond K.P. & van de Kamp P.C., 1984: Diagenetic mineralogy and controls on albitization and laumontite formation in Paleogene arkoses, Santa Ynez Mountains, California. In: McDonald D.A. & Surdam D.C. (Eds.): Clastic Diagenesis. *Amer. Assoc. Petrol. Geol. Mem.*, 37, 239–276.

Hillier S., 1993: Origin, diagenesis, and mineralogy of chlorite minerals in Devonian lacustrine mudrocks, Orcadian Basin, Scotland. *Clays and Clay Miner.*, 41, 240–259.

Hillier S., 1995: Mafic phyllosilicates in low-grade metabasites. Characterization using deconvolution analysis — discussion. *Clay Miner.*, 30, 67–73.

Iijima A. & Utada M., 1971: Present-day diagenesis of the Neogene geosynclinal deposits in the Niigata oilfield, Japan. In: Gould R.F. (Ed.): *Molecular sieve zeolites-I (Advances in chemistry, Series 101). Amer. Chem. Soc.*, Washington DC, 34–349.

Inoue A., Utada M., Nagata H. & Watanabe T., 1984: Conversion of trioctahedral smectite to interstratified chlorite/smectite in Pliocene acidic pyroclastic sediments of the Ohyiu district, Akita Prefecture, Japan. *Clay Sci.*, 6, 103–116.

Inoue A. & Utada M., 1991: Smectite-to-chlorite transformation in thermally metamorphosed volcanoclastistic rocks in the Kamikita area, northern Honshu, Japan. *Amer. Mineralogist*, 76, 628–640.

Jackson M.L., 1975: Soil chemical analysis — advanced course. *Madison,* Wisconsin, 1–386.

Janks J.S., Yusas M.R. & Hall C.M., 1992: Clay mineralogy of the interbedded sandstone, dolomite, and anhydrite: The Permian Yates Formation, Winkler County, Texas. In: Houseknecht D.W. & Pittman E.D. (Eds.): *Origin, diagenesis, and petrophysics of clay minerals in sandstones. SEPM Spec. Publ.,* 47, 145–157.

Kristmannsdóttir H., 1979: Alteration of basaltic rocks by hydrothermal activity at 100–300 °C. In: Mortland M.M. & Farmer V.C. (Eds.): *Proc. Int. Clay Confer. 1978, Elsevier*, Amsterdam, 359–367.

MacEwan D.M.C. & Wilson M.J., 1980: Interlayer and intercalation complexes of clay minerals. In: Brindley G.W. & Brown G. (Eds.): Crystal structures of clay minerals and their X-ray identification. *Mineral. Soc.*, *(London),* 197–249.

Malla P.B. & Douglas L.A., 1987: Identification of expanding layer silicates: Layer charge vs. expansion properties. *Proc. Int. Clay Confer. 1985, Denver.*, *Clay Miner. Soc*., Bloomington, Indiana, 85–96.

Masaryk P., Šucha V. & Lintnerová O., 1995: Is the volcanic material present in the Middle Triassic basin sediments of the Hronic Unit (Choč Nappe, Western Carpathians)? *Geol. Carpathica*, 46, 175–181.

Meunier A., Inoue A. & Beaufort D., 1991: Chemographic analysis of trioctahedral smectite-to-chlorite conversion series from the Ohyu caldera, Japan. *Clays and Clay Miner.*, 39, 409–415.

Moraes M.A.S. & de Ros L.F., 1992: Depositional, infiltrated and authigenic clays in fluvial sandstones of the Jurassic Sergi Formation, Recôncavo Basin, northeastern Brazil. In: Houseknecht D.W. & Pittman E.D. (Eds.): *Origin, diagenesis, and petrophysics of clay minerals in sandstones. SEPM Spec. Publ.,* 47, 197–208.

Reynolds R.C., 1980: Interstratified clay minerals. In: Brindley G.W. & Brown G. (Eds.): Crystal Structures of Clay Minerals and their X-ray Identification. *Mineral. Soc.*, *(London)*, 249–303.

Reynolds R.C., 1985: NEWMOD A computer program for the calculation of the one-dimensional patterns of mixed-layered clays. *R.C. Reynolds, 8 Brook Rd.* Hanover, New Hampshire.

Reynolds R.C., 1988: Mixed layer chlorite minerals. In: Bailey S.W. (Ed.): *Hydrous phyllosilicates (exclusive of micas). Rev. in Mineralogy, Vol. 19*, *Miner. Soc. Amer.*, 601–629.

Robinson D., Bevins R.E. & Rowbotham G., 1993: The characterization of mafic phyllosilicates in low-grade metabasalts from eastern Greenland. *Amer. Mineralogist*, 78, 377–390.

Schiffman P. & Fridleifsson G.O., 1991: The smectite-chlorite transition in drillhole NJ-15 Nesjavellir geothermal field, Iceland: XRD, BSE, and electron microprobe investigations. *J. Metamorphic Geol.*, 9, 679–696.

Schiffman P. & Stautigel H., 1995: The smectite to chlorite transition in a fossil seamount hydrothermal system: The basement complex of La Palma, Canary Islands. *J. Metamorphic Geol.*,

13, 487–498.

Schiffman P. & Southard R.J., 1996: Cation exchange capacity of layer silicates and palagonitized glass in mafic volcanic rocks: A comparative study of bulk extraction and *in situ* techniques. *Clays and Clay Miner.*, 44, 624–634.

Schultz L.G., 1963: Clay minerals in the Triassic rocks of the Colorado Plateau. *U.S. Geol. Surv. Bull*., 1147-C, 1–71.

Shau Y.H., Peacor D.R. & Essene E.J., 1990: Corrensite and mixed-layer chlorite/corrensite in metabasalts from northern Taiwan: TEM/AEM, EMPA, XRD, and optical studies. *Contr. Mineral. Petrology*, 105, 123–142.

Shau Y.H. & Peacor D.R., 1992: Phyllosilicates in hydrothermally altered basalts from DSDP Hole 504B, Leg 83 — a TEM and AEM study. *Contr. Mineral. Petrology*, 112, 119–133.

Soták J. & Bebej J., 1996: Serpentinitic sandstones from the Šambron-Kamenica Zone in Eastern Slovakia: Evidence of deposition in a Tertiary collisional belt. *Geol. Carpathica,* 47, 227–239.

Velde B., 1977: Clays and clay minerals in natural and synthetic systems. *Elsevier*, Amsterdam, 1–211.

Wilson M.D. & Pittman E.D., 1977: Authigenic clays in sandstones: Recognition and influence on reservoir properties and paleoenvironmental analysis. *J. Sed. Petrology*, 47, 3–31.

Wintsch R.P. & Kvale C.M., 1994: Differential mobility of elements in burial diagenesis of siliciclastic rocks. *J. Sed. Res.*, A64, 349–361.